Memory Effect in a Topological Surface State of Bi_2Te_2Se

Ying-Shuang Fu,[†,*] Tetsuo Hanaguri,[†,‖] Shuhei Yamamoto,[‡] Kyushiro Igarashi,[‡] Hidenori Takagi,[§,⊥] and Takao Sasagawa[‡]

[†]RIKEN Center for Emergent Matter Science, Wako, Saitama 351-0198, Japan, [‡]Materials and Structures Laboratory, Tokyo Institute of Technology, Yokohama, Kanagawa 226-8503, Japan, [§]RIKEN Magnetic Materials Laboratory, Wako, Saitama 351-0198, Japan, [⊥]Department of Physics, University of Tokyo, Bunkyo-ku, Tokyo 113-0033, Japan. [‖]E-mail address: hanaguri@riken.jp.

ABSTRACT We demonstrate the controllable local manipulation of the Dirac surface state in a topological insulator, Bi_2Te_2Se, which has suppressed bulk carrier density. Using scanning tunneling microscopy/spectroscopy under magnetic fields, we observe Landau levels of the Dirac surface state in the conductance spectra. The Landau levels start to shift in their energy once the bias voltage between the tip and the sample exceeds a threshold value. The amount of shift depends on the history of bias ramping. As a result, conductance spectra show noticeable hysteresis, giving rise to a memory effect. The conductance images exhibit spatially inhomogeneous patterns which can also be controlled by the bias voltage in a reproducible way. On the basis of these observations, we argue that the memory effect is associated with the tip-induced local charging effect which is pinned by the defect-generated random potential. Our study opens up a new avenue to controlling the topological surface state.

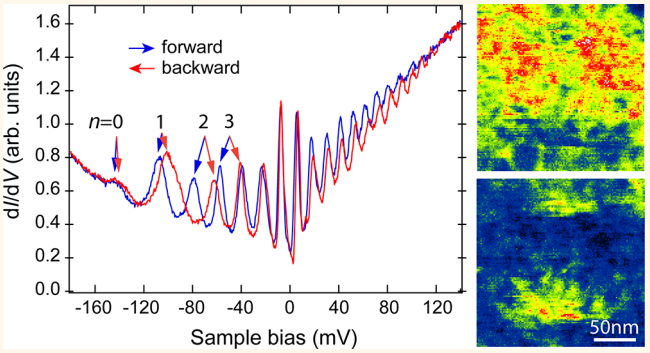

KEYWORDS: topological insulator · Bi_2Te_2Se · Landau level · hysteresis · STM

Topological insulators (TI) are the hallmark of a new quantum material featured by an insulating gap in the bulk and a metallic topological surface state (TSS) with Dirac-cone-like dispersion at the surface boundary.[1,2] Topological nature is induced by strong spin−orbit interaction which locks the spin and momentum of electrons in the TSS, making electrons propagating at opposite directions possess opposite spin orientations. As a result, any time-reversal invariant perturbations do not cause backscattering in the TSS, which is highly desirable for application in dissipationless spintronics. In addition, TSS may host novel excitations when in proximity with magnetism[3,4] or superconductivity,[5,6] which provide platforms for revealing yet more exotic physics and applications.

A prerequisite of using TI for various applications and unraveling novel physics is to control the TSS. However, actual strong three-dimensional topological insulators such as Bi_2Te_3, Bi_2Se_3, and Sb_2Te_3 are heavily doped by various defects that are unavoidably generated during crystal growth.[7−10] As a result, bulk carriers dominate electronic transport properties and hinder electrical tuning of TSS effectively. Various approaches have been employed to reduce the bulk carrier density, including impurity doping,[9−12] epitaxial growth,[13−15] compositional engineering,[16−20] *etc.*

Actual materials include not only bulk carriers but also various categories of disorders. Although the TSS is protected against backscattering even in the presence of disorder, electronic states of the TSS should be inhomogeneous as affected by charged defects. Indeed, recent scanning tunneling microscopy/spectroscopy (STM/STS) studies on intentionally doped Bi_2Se_3 and Bi_2Te_3 have revealed "charge puddles" associated with the disorder.[21]

Although disorder is generally a foe to applications, here we show that it provides us with a unique opportunity to manipulate the TSS so long as the bulk carrier density is reduced. Our technique is STM/STS which can be used not only to image the electronic

* Address correspondence to yfu@riken.jp.

Received for review January 24, 2013 and accepted April 7, 2013.

Published online April 07, 2013
10.1021/nn400378f

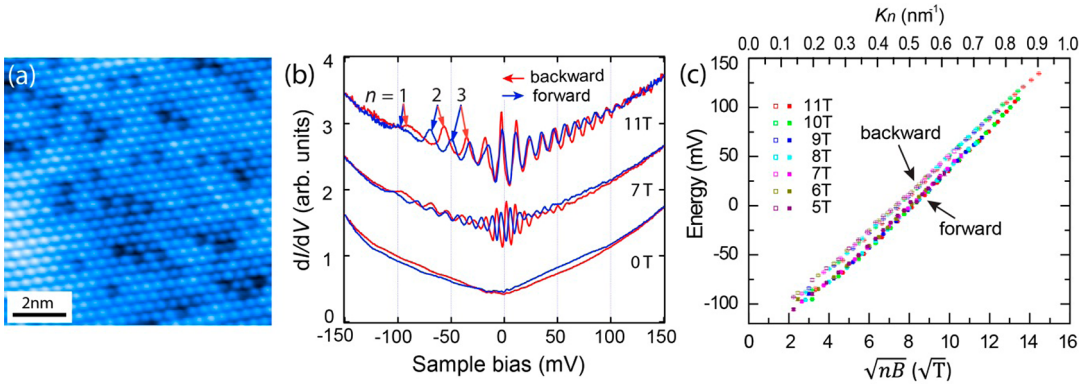

Figure 1. LL spectra of Bi_2Te_2Se. (a) High-resolution STM image showing the topography of the Bi_2Te_2Se surface. Imaging condition: sample bias voltage $V = -50$ mV and tunneling current $I = 33.1$ pA. (b) Tunneling spectra of the Bi_2Te_2Se surface, showing the emergence of LL states after a magnetic field is applied. The spectra of the TSS exhibit hysteresis between the forward (blue curves) and backward (red curves) branches. The LL indexes are marked. Tunneling gap was set at $V = -50$ mV and $I = 33.1$ pA. Spectra under the fields are offset vertically. The spectra were taken between -250 and $+250$ mV, and only part of the curves within ± 150 mV is shown for clarity. (c) Scaling plot of the energy of LLs *versus* $(nB)^{1/2}$, which is proportional to the electron momentum k as shown in the top axis.[27] LL energies for the forward and backward branches are marked with solid and hollow squares, respectively.

inhomogeneity but also to modify the electronic state *via* the local probe gating. We study Bi_2Te_2Se which is a prototypical TI synthesized from compositional engineering. It has a quintuple-layer unit of Te−Bi−Se−Bi−Te, forming a well-ordered tetradymite structure. Since the isostructural materials Bi_2Te_3 and Bi_2Se_3 are hole-doped and electron-doped, respectively, Bi_2Te_2Se has a suppressed bulk carrier concentration.[16,17] In comparison to Bi_2Se_3, its Fermi level is moved below the conduction band minimum as evidenced from both angle-resolved photoemission spectroscopy (ARPES)[22−24] and transport measurements.[16,17,25]

STM/STS experiments have been done under a magnetic field, where Landau levels (LLs) can be used as an energy marker of electrons in the TSS. We found that the tunneling-conductance image is spatially inhomogeneous, invoking the importance of disorder. Intriguingly, the LL spectrum as a function of bias voltage exhibits a clear hysteresis loop. As a result, the conductance image shows different patterns even at the same energy depending on the history of bias voltage ramping. We argue this memory effect in the framework of charge redistribution as induced by local probe gating in conjunction with its pinning by disorder.

RESULTS AND DISCUSSION

Figure 1a shows a high-resolution STM image of the cleaved Bi_2Te_2Se surface, where the ordered triangular lattice is clearly resolved. Its lattice constant is estimated to be 4.2 Å, which is consistent with the bulk value. Since cleaving occurs between the adjacent Te layers, the imaged atoms should all be Te. However, a large number of atoms with reduced height can be clearly seen. We attribute them to the Se atoms which substitute the Te sites, as Se has a smaller atomic radius than Te. A similar defect has also been reported in ref 26. The STS spectra taken at the smaller atoms show no obvious difference from those at other defect-free areas, suggesting that they share the same valence charge state as Te. This further substantiates the present assignment.

Unexpectedly, a clear hysteresis is observed in the tunneling spectra (Figure 1b) between different bias ramping directions. After magnetic field is applied, discrete peaks that are ascribed to LL states emerge whose energy spacing increases with strength of magnetic field (Figure 1b).[27−30] The conductance hysteresis of the TSS is more evidently manifested from the LL spectra, where the LL states could clearly mark the energy shift. The LL states of a two-dimensional Dirac fermion system obey the following relation: $E_n = E_D + \mathrm{sgn}(n)v(2e\hbar|n|B)^{1/2}$, $n = 0, \pm1, \pm2,...$, where n is LL index, E_n is the energy location of the nth LL state, E_D is Dirac point energy, B is magnetic field, and v is the velocity of the electron. We fit the energy location of LL states with a series of Gaussian peaks. After their energies being plotted as a function of $(|n|B)^{1/2}$, all of the data are scaled to two curves (Figure 1c), corresponding to the forward and backward branches, respectively. (The forward direction is defined as a voltage ramping from negative to positive bias.) In the intermediate and small bias range, the two branches show similar energy dispersions but shift rigidly about 13.5 meV relative to each other. However, at large bias regimes, they exhibit deviated dispersions and finally overlap close to the limits of ramping bias, which reflects the intrinsic LL energies being perturbed by applied bias. The intensity of zeroth LL is found to be strongly suppressed as compared to that in Bi_2Se_3.[31] The weak intensity of the zeroth LL state is probably related to the band structure[32] of the Bi_2Te_2Se where the Dirac point is slightly below the valence band

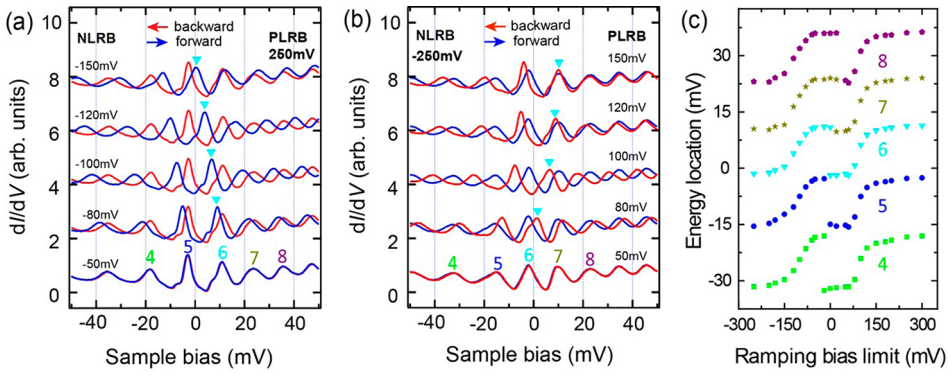

Figure 2. Hysteresis of LL states with ramping bias limit. (a,b) LL spectra of Bi_2Te_2Se at 11 T, showing the shifting of LL states with different limits of ramping bias. In panel a (b), the spectra were initialized at a fixed PLRB (NLRB) of + (−) 250 mV, and their NLRBs (PLRBs) are varied as indicated. The forward (backward) bias ramping directions are marked with blue (red) arrows. For clarity, only part of the data between ±50 mV is shown, and its view with larger energy window is presented in Figure S3 of Supporting Information. The energy positions of LL states are stationary when the bias is ramped from the initialized bias to the indicated ramping bias limits and shift when ramped back. Energy positions the of sixth LL state are marked with aqua triangles to representatively indicate the shifting of LL states. The energy locations of fourth to eighth LL states are marked, whose statistics of shifting with ramping bias limit are plotted in (c), exhibiting clear hysteresis loops. All of the spectra were collected with the tunneling gap set at $V = -50$ mV and $I = 33.1$ pA.

maximum (Supporting Information Figure S1b), which may obscure the LL states.[27]

The shifted LLs indicate that carrier density of the Dirac surface state changes between forward and backward branches. Surface electron density N_s can be calculated using Fermi momentum k_F as $N_s = k_F^2/4\pi$. Since the scaling variable $(|n|B)^{1/2}$ is proportional to momentum,[27] k_F can be obtained from the scaling function shown in Figure 1c, which represents the energy-momentum dispersion relation.[27] The estimated N_s values are $\sim 1.6 \times 10^{12}$ and $\sim 1.3 \times 10^{12}$ cm^{-2} for the two respective branches, which then differs by $\sim 0.3 \times 10^{12}$ cm^{-2}. These are indeed lower than that of high-quality Bi_2Se_3 which is calculated as $\sim 3.5 \times 10^{12}$ cm^{-2}.[27]

To study the hysteresis behavior in detail, we systematically change the limits of ramping bias and characterize the consequent response of LL shift at 11 T. We first fix the positive limit of ramping bias (PLRB) at +250 mV and vary the negative limit of ramping bias (NLRB). As is shown in Figure 2a, when the sample bias is ramped from the fixed PLRB to the varying NLRB (red curves), the energy positions of LL states are all unchanged, indicating that they are determined by the PLRB of +250 mV. However, when the bias is ramped back, the LL states shift to the negative bias direction progressively with the increasing magnitude of NLRB (Figure 2a, blue curves), as is representatively indicated with aqua triangles on the sixth LL peak. The LL shifting is activated when the NLRB exceeds the threshold value of about −60 mV and gradually saturates after NLRB is over about −180 mV. A similar shifting behavior also occurs for the opposite bias polarity with the LL spectra initialized at a fixed NLRB of −250 mV (Figure 2b): The LL energies are always stationary when the bias is ramped from the fixed NLRB to different PLRB (blue curves) but shift to the positive bias direction when ramped back with the increasing magnitude of PLRB (Figure 2b, red curves). In this case, threshold and saturation PLRBs are +60 and ∼+150 mV, respectively.

After the spectra in Figure 2a,b were fitted with multiple Gaussian peaks, energy positions of the fourth to eighth LL states as a function of ramping bias limit were plotted in Figure 2c. They all exhibit clear hysteresis loops[33] with similar size, demonstrating that they together shift rigidly. The amount of LL shifting is 13.1 ± 0.6 meV when the PLRB and NLRB are +250 and −250 mV, respectively. The rigid shift in LL energies seen in Figure 1c and Figure 2c invokes the following phenomenology. The biased tip modifies the potential energy for surface Dirac electrons, and the modified potential has a memory effect on the history of the ramping bias. This renders it feasible to manipulate the TSS. To demonstrate this capability, we position the tip at the same location, initialize the LL spectra with different voltage settings, and then check the energy positions of LL states in a low-energy range below the thresholds (bias voltage <±60 mV). The top curve in Figure 3a shows a spectrum taken after the spectra being set at −200 mV. They rigidly shift to positive bias directions after a +200 mV setting (middle curve in Figure 3a). As is representatively indicated with the sixth LL state marked with aqua triangle, it shifts from −1.9 to 11.5 meV, which is consistent with Figure 2c. With another voltage setting at −200 mV, the LL states shift back to their original energy positions and the sixth LL state locates at −0.8 meV, indicating that the conductance manipulation is reversible.

We further examine the dynamic properties of the controlled LL shifting. We found that the LL hysteresis has negligible dependence on the speed of bias sweep between 0.14 and 0.014 V/s (Supporting Information, Figure S3). This demonstrates that the potential energy

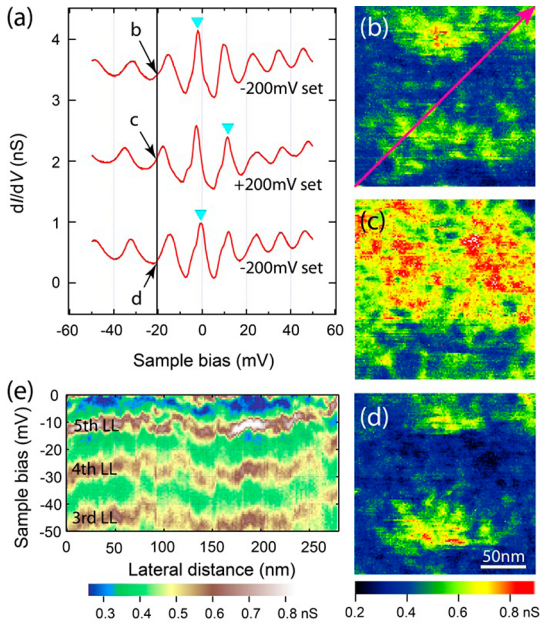

Figure 3. Manipulation of the LL states. (a) LL states of Bi_2Te_2Se at 11 T after being set with different voltages indicated by the curves. All LLs shift rigidly in energy, so the sixth LL state (aqua triangle) can representatively indicate their shifting. All of the spectra were collected with the tunneling gap set at $V = -50$ mV, $I = 33.1$ pA and sequentially offset the middle and upper curves by 1 nS. After each manipulation, a sample voltage of -21 mV (marked with a black line in (a)) was selected to map the conductance change of the surrounding area. The manipulated location is at the image center (b–d). (e) Intensity plot of d*I*/d*V* spectra taken along a marked red line in (b) showing the spatial fluctuation of the LL states. The LL indexes are marked.

for surface Dirac electrons reorganizes to reach energy equilibriums on the order of ~0.1 eV/s or even faster. We also studied the stability of the shifted LL states after the setting. If the system is set at positive bias voltage, we did not observe any change in the spectra even after a day, as long as the bias voltage is kept within ±60 mV. After the negative voltage setting, an energy decay of LL spectra was observed at some locations, while the spectra stay stationary in other locations such as where the spectra in Figure 3a were taken. Even at the location where the fastest decay was observed, change in the spectrum evolves in a time scale on the order of hours (Supporting Information, Figure S4).

Next we did real space spectroscopic imaging to unravel the physical mechanism behind the conductance hysteresis phenomena. Figure 3b–d shows differential conductance maps of the same area (scanning size: 200 nm × 200 nm) all taken at −21 mV after different voltage settings. All settings were done at the center of the field of view, and the spectra in Figure 3a were also taken at the same location. After a −200 mV setting, the conductance map exhibits depressed intensity around the central location (Figure 3b). Its contrast changes after being set at +200 mV (Figure 3c), which now displays high intensity at the central area. This corresponds well to the point spectra shown in Figure 3a; that is, the imaging energy of −21 mV is close to the peak position of fourth LL when the spectra are set at +200 mV, while it is between the fourth and fifth LLs when set at −200 mV. Importantly, the intensity can be reversed back to the original contrast (though not exactly identical) after another −200 mV setting again (Figure 3d), which is also consistent with the point spectra in Figure 3a.

There are two aspects revealed from the conductance mappings. For one thing, the contrast change reflects that the spatial energy landscape surrounding the tip is modified by the voltage setting. Since the setting effect extends over the whole field of view, it is not induced by the tunneling current which is limited within an atomic scale, but may be related to the electric field exerted by the biased tip. In order to estimate the spatial extent, we consider a minimal model in which an irreversible electronic state change occurs when the tip-induced electric field exceeds a local critical value. By approximating that the sample is a perfect conductor and the tip apex is a hemisphere with a radius of r_0, we calculated the lower limit of the diameter of the affected area as $\sim 2.4r_0$, using the observed critical voltage of 60 mV and the setting bias voltage of 200 mV. Since the typical tip radius is about a few tens of nanometers, the spatial influence should extend at least on the order of several tens of nanometers. If the effects of irreversible charge redistribution and finite conductance are taken into account, the spatial extent should become larger as observed. The detailed spatial extent of the setting effect is an interesting future issue.

For another aspect, LL energies exhibit spatial variation. For an example, we show position-dependent LL spectra in Figure 3e. A spatial fluctuation of LL energy is on the order of 10 meV, which corresponds to the N_s variation of $\sim 0.2 \times 10^{12}$ cm^{-2}. The fluctuation of LL energy is about the same size as the irreversible shift of LL energy after setting, suggesting the relation between them. The major source of the electronic inhomogeneity may come from underlying Bi/Te antisite defects,[23,26] which are heterovalent and act as charge donors, instead of the isovalent Te/Se antisite defects manifested in Figure 1a. Regardless of their origin, impurity charges in Bi_2Te_2Se should be poorly screened due to the reduced carrier density, causing profound variations of the real space potential landscape.[34] It is interesting to note that LLs are well-defined even in such an inhomogeneous electronic background.

On the basis of the above observations and analyses, we argue the possible origin of the conductance hysteresis. When tunneling spectroscopy is performed to a bulk insulating TI surface, screening of the biased tip involves movement of surface carriers, inducing

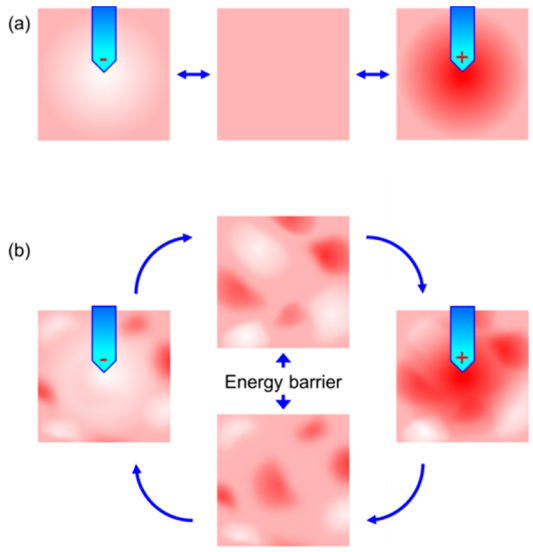

Figure 4. Two-dimensional electronic state change induced by a biased tip in homogeneous (a) and inhomogeneous (b) systems. Schematics show the distribution patterns of energy potential, *i.e.*, Dirac point energy. Darker color means deeper potential or that more electrons are there. Polarity of the tip bias is indicated on the tip and is opposite to that of the sample bias. If the system is homogeneous, the effect of band bending is reversible. In a system with disorder, there are different metastable potential distribution patterns with a similar system's total energy, and they are separated by the energy barrier. When tip-induced change in the local electron density is high enough, potential distribution patterns can change from one metastable state to another.

significant local band bending under the tip.[28] The local band is bent downward/upward in the presence of a positively/negatively biased tip relative to the sample (Figure 4a,b), which affects the energy position of the TSS measured by tunneling spectroscopy. In a spatially homogeneous TI, charge carriers move smoothly with the local band bending, and there is a one-to-one correspondence between the charge distribution pattern and the applied bias voltage. In other words, no hysteresis is expected.

However, in a disordered system as in Bi_2Te_2Se, a charge distribution pattern would not be uniquely determined even at the same bias voltage because there would be different metastable patterns separated by the energy barrier for the system's total energy. If the bias voltage-induced potential deformation is small, the original pattern should be intact as protected by the energy barrier. However, once the potential deformation becomes large enough to overcome the energy barrier, the irreversible charge redistribution should occur. The resultant pattern is again protected by the energy barrier unless the tip is biased with a large enough voltage (Figure 4b). In order to achieve this irreversible charge redistribution, the tip-induced charge density should be larger than (or at least as large as) the spatial fluctuation of charge density. The tip-induced charge density in the bulk insulating sample can be roughly approximated by $\varepsilon_0 V/d$,[28] where ε_0 is vacuum permittivity and $d \sim 1$ nm is the tip−sample distance. At the observed critical bias voltage of 60 mV, the induced electron density is estimated to be $\sim 0.3 \times 10^{12}$ cm^{-2}, consistent with the fluctuation of N_s as well as the rigid shift of LL energy after the setting. In this way, the observed conductance hysteresis in Bi_2Te_2Se can be explained by the tip-induced local band bending pinned by the defect-induced disorder.

CONCLUSION

In summary, we have characterized the prototypical TI Bi_2Te_2Se with STM/STS technique and found electronic inhomogeneity present in the commonly believed stoichiometric compound. By courtesy of LL spectra, we demonstrated that the conductance of the TSS exhibits hysteresis loops as driven by the interplay between the local probe gating and the defect-induced disorder. This provides a novel approach for controlling the TSS, which could be generally applied to other carrier-compensated TIs possessing disorder. Since the potential landscape can be modified with local probe gating, this paves the way for future studies of LL physics in the presence of a controlled potential.[30,35] Extensions to other applications can be envisioned such as locally gating the conductance of TSS for information storage and conductance patterning on the TI surface for building various nanoelectric and spintronic devices.

EXPERIMENTAL DETAILS

Bi_2Te_2Se crystals were grown by a modified Bridgman technique, which has been established for the growth of pure and impurity-doped Bi_2Se_3 crystals.[4] All measurements were performed at 1.5 K with a modified UNISOKU ultrahigh vacuum (UHV) ($<1 \times 10^{-10}$ Torr) low-temperature STM which is equipped with a high-field magnet.[36] Magnetic field up to 11 T can be applied perpendicular to the sample surface. Bi_2Te_2Se crystal was cleaved *in situ* under UHV conditions at ~77 K. After cleaving, the crystal was transferred quickly to the low-temperature STM for subsequent measurements. An *ex situ* electrochemically etched polycrystalline tungsten tip was used as the STM probe. It has been cleaned and characterized *in situ* with a field-ion microscope (FIM) until well-defined images of concentric rings coming from tungsten atoms around the tip apex are obtained. The imaging gas was helium with a pressure of 2×10^{-5} Torr. After FIM treatment, the tip routinely guarantees tunneling spectra free from tip-related features. Tunneling spectra were recorded by utilizing a lock-in detection of the tunneling current with an AC modulation voltage of 1.4 mV_{rms} at 617.3 Hz feeding into the sample bias. The feedback loop was off during spectra acquisition. The tip is grounded as the reference voltage. In total, four different samples were investigated to confirm the reproducibility of the measurement results.

Conflict of Interest: The authors declare no competing financial interest.

Acknowledgment. The authors are indebted to Y. Kohsaka for helpful discussions and technical assistance in data analysis.

This work is funded by Grant-in-Aid for Scientific Research from the Ministry of Education, Culture, Sports, Science and Technology of Japan. Y.F. acknowledges additional support from a RIKEN Foreign Postdoctoral Researcher (FPR) fellowship.

Supporting Information Available: Additional STS data showing the resolvable zeroth LL state and a schematic band structure of Bi_2Te_2Se, hysteresis of LL states with different ramping bias limit at large energy window, hysteresis of LL states irrelevant to bias ramping speed, and stability of the shifted LL states with time. This material is available free of charge *via* the Internet at http://pubs.acs.org.

REFERENCES AND NOTES

1. Qi, X. L.; Zhang, S. C. Topological Insulators and Superconductors. *Rev. Mod. Phys.* **2011**, *83*, 1057–1110.
2. Hasan, M. Z.; Kane, C. L. Colloquium: Topological Insulators. *Rev. Mod. Phys.* **2010**, *82*, 3045.
3. Qi, X. L.; Li, R.; Zhang, J.; Zhang, S. C. Inducing a Magnetic Monopole with Topological Surface States. *Science* **2009**, *323*, 1184–1187.
4. Chen, Y. L.; Chu, J.-H.; Analytis, J. G.; Liu, Z. K.; Igarashi, K.; Kuo, H.-H.; Qi, X. L.; Mo, S. K.; Moore, R. G.; Lu, D. H.; *et al.* Massive Dirac Fermion on the Surface of a Magnetically Doped Topological Insulator. *Science* **2010**, *329*, 659–662.
5. Fu, L.; Kane, C. L. Superconducting Proximity Effect and Majorana Fermions at the Surface of a Topological Insulator. *Phys. Rev. Lett.* **2008**, *100*, 096407.
6. Qi, X. L.; Hughes, T. L.; Raghu, S.; Zhang, S. C. Time-Reversal-Invariant Topological Superconductors and Superfluids in Two and Three Dimensions. *Phys. Rev. Lett.* **2009**, *102*, 187001.
7. Xia, Y.; Qian, D.; Hsieh, D.; Wray, L.; Pal, A.; Lin, H.; Bansil, A.; Grauer, D.; Hor, Y. S.; Cava, R. J.; *et al.* Observation of a Large-Gap Topological-Insulator Class with a Single Dirac Cone on the Surface. *Nat. Phys.* **2009**, *5*, 398–402.
8. Hsieh, D.; Xia, Y.; Qian, D.; Wray, L.; Meier, F.; Dil, J. H.; Osterwalder, J.; Patthey, L.; Fedorov, A. V.; Lin, H.; *et al.* Observation of Time-Reversal-Protected Single-Dirac-Cone Topological-Insulator States in Bi_2Te_3 and Sb_2Te_3. *Phys. Rev. Lett.* **2009**, *103*, 146401.
9. Chen, Y. L.; Analytis, J. G.; Chu, J. H.; Liu, Z. K.; Mo, S. K.; Qi, X. L.; Zhang, H. J.; Lu, D. H.; Dai, X.; Fang, Z.; *et al.* Experimental Realization of a Three-Dimensional Topological Insulator Bi_2Te_3. *Science* **2009**, *325*, 178–181.
10. Hsieh, D.; Xia, Y.; Qian, D.; Wray, L.; Dil, J. H.; Meier, F.; Osterwalder, J.; Patthey, L.; Checkelsky, J. G.; Ong, N. P.; *et al.* A Tunable Topological Insulator in the Spin Helical Dirac Transport Regime. *Nature* **2009**, *460*, 1101–1105.
11. Wang, Y.; Xiu, F.; Cheng, L.; He, L.; Lang, M.; Tang, J.; Kou, X.; Yu, X.; Jiang, X.; Chen, Z.; *et al.* Gate-Controlled Surface Conduction in Na-Doped Bi_2Te_3 Topological Insulator Nanoplates. *Nano Lett.* **2012**, *12*, 1170–1175.
12. Analytis, J. G.; McDonald, R. D.; Riggs, S. C.; Chu, J.-H.; Boebinger, G. S.; Fisher, I. R. Two-Dimensional Surface State in the Quantum Limit of a Topological Insulator. *Nat. Phys.* **2010**, *6*, 960–964.
13. Chen, X.; Ma, X. C.; He, K.; Jia, J. F.; Xue, Q. K. Molecular Beam Epitaxial Growth of Topological Insulators. *Adv. Mater.* **2011**, *23*, 1162–1165.
14. He, L.; Xiu, F.; Yu, X.; Teague, M.; Jiang, W.; Fan, Y.; Kou, X.; Lang, M.; Wang, Y.; Huang, G.; *et al.* Surface-Dominated Conduction in a 6 nm thick Bi_2Se_3 Thin Film. *Nano Lett.* **2012**, *12*, 1486–1490.
15. Jiang, Y. P.; Sun, Y. Y.; Chen, M.; Wang, Y. L.; Li, Z.; Song, C. L.; He, K.; Wang, L. L.; Chen, X.; Xue, Q. K.; *et al.* Fermi-Level Tuning of Epitaxial Sb_2Te_3 Thin Films on Graphene by Regulating Intrinsic Defects and Substrate Transfer Doping. *Phys. Rev. Lett.* **2012**, *108*, 066809.
16. Ren, Z.; Taskin, A. A.; Sasaki, S.; Segawa, K.; Ando, Y. Large Bulk Resistivity and Surface Quantum Oscillations in the Topological Insulator Bi_2Te_2Se. *Phys. Rev. B* **2010**, *82*, 241306(R).
17. Jia, S.; Ji, H.; Climent-Pascual, E.; Fuccillo, M. K.; Charles, M. E.; Xiong, J.; Ong, O. P.; Cava, R. J. Low-Carrier-Concentration Crystals of the Topological Insulator Bi_2Te_2Se. *Phys. Rev. B* **2011**, *84*, 235206.
18. Kong, D.; Chen, Y.; Cha, J. J.; Zhang, Q.; Analytis, J. G.; Lai, K.; Liu, Z.; Hong, S. S.; Koski, K. J.; Mo, S. K.; *et al.* Ambipolar Feld Effect in the Ternary Topological Insulator $(Bi_xSb_{1-x})_2Te_3$ by Composition Tuning. *Nat. Nanotechnol.* **2011**, *6*, 705.
19. Zhang, J.; Chang, C.; Zhang, Z.; Wen, J.; Feng, X.; Li, K.; Liu, M.; He, K.; Wang, L.; Chen, X.; *et al.* Band Structure Engineering in $(Bi_{1-x}Sb_x)_2Te_3$ Ternary Topological Insulators. *Nat. Commun.* **2011**, *2*, 574.
20. Hong, S. S.; Cha, J. J.; Kong, D.; Cui, Y. Ultra-low Carrier Concentration and Surface-Dominant Transport in Antimony-Doped Bi_2Se_3 Topological Insulator Nanoribbons. *Nat. Commun.* **2012**, *3*, 757.
21. Beidenkopf, H.; Roushan, P.; Seo, J.; Gorman, L.; Drozdov, I.; Hor, Y. S.; Cava, R. J.; Yazdani, A. Spatial Fluctuations of Helical Dirac Fermions on the Surface of Topological Insulators. *Nat. Phys.* **2011**, *7*, 939.
22. Arakane, T.; Sato, T.; Souma, S.; Kosaka, K.; Nakayama, K.; Komatsu, M.; Takahashi, T.; Ren, Z.; Segawa, K.; Ando, Y. Tunable Dirac Cone in the Topological Insulator $Bi_{2-x}Sb_xTe_{3-y}Se_y$. *Nat. Commun.* **2012**, *3*, 636.
23. Scanlon, D. O.; King, P. D. C.; Singh, R. P.; de la Torre, A.; Walker, S. M.; Balakrishnan, G.; Baumberger, F.; Catlow, C. R. A. Controlling Bulk Conductivity in Topological Insulators: Key Role of Anti-site Defects. *Adv. Mater.* **2012**, *24*, 2154–2158.
24. Neupane, M.; Xu, S. Y.; Wray, L. A.; Petersen, A.; Shankar, R.; Alidoust, N.; Liu, C.; Fedorov, A.; Ji, H.; Allred, J. M.; *et al.* Topological Surface States and Dirac Point Tuning in Ternary Topological Insulators. *Phys. Rev. B* **2012**, *85*, 235406.
25. Xiong, J.; Luo, Y.; Khoo, Y.; Jia, S.; Cava, R. J.; Ong, N. P. High-Field Shubnikov−de Haas Oscillations in the Topological Insulator Bi_2Te_2Se. *Phys. Rev. B* **2012**, *86*, 045314.
26. Jia, S.; Beidenkopf, H.; Drozdov, I.; Fuccillo, M. K.; Seo, J.; Xiong, J.; Ong, N. P.; Yazdani, A.; Cava, R. J. Defects and High Bulk Resistivities in the Bi-Rrich Tetradymite Topological Insulator $Bi_{2+x}Te_{2-x}Se$. *Phys. Rev. B* **2012**, *86*, 165119.
27. Hanaguri, T.; Igarashi, K.; Kawamura, M.; Takagi, H.; Sasagawa, T. Momentum-Resolved Landau-Level Spectroscopy of Dirac Surface State in Bi_2Se_3. *Phys. Rev. B* **2010**, *82*, 081305(R).
28. Cheng, P.; Song, C.; Zhang, T.; Zhang, Y.; Wang, Y.; Jia, J.; Wang, J.; Wang, Y.; Zhu, B.; Chen, X.; *et al.* Landau Quantization of Topological Surface States in Bi_2Se_3. *Phys. Rev. Lett.* **2010**, *105*, 076801.
29. Jiang, Y. P.; Wang, Y. L.; Chen, M.; Li, Z.; Song, C. L.; He, K.; Wang, L. L.; Chen, X.; Ma, X. C.; Xue, Q. K. Landau Quantization and the Thickness Limit of Topological Insulator Thin Films of Sb_2Te_3. *Phys. Rev. Lett.* **2012**, *108*, 016401.
30. Okada, Y.; Zhou, W.; Dhital, C.; Walkup, D.; Ran, Y.; Wang, X.; Wilson, S. D.; Madhavan, V. Visualizing Landau Levels of Dirac Electrons in a One-Dimensional Potential. *Phys. Rev. Lett.* **2012**, *109*, 066407.
31. The zeroth LL is barely resolvable in the spectra of Figure 1b but is observable though weak in other locations of the sample. See Supporting Information, Figure S1.
32. Lin, H.; Das, T.; Wray, L. A.; Xu, S. Y.; Hasan, M. Z.; Bansil, A. An Isolated Dirac Cone on the Surface of Ternary Tetradymite-like Topological Insulators. *New J. Phys.* **2011**, *13*, 095005.
33. It is noted that the hysteresis loops in Figure 2c are not closed, where the parts expected to show the LL states unchanged with the ramping bias limit are missing. This is due to the fact that under those occasions the ramping biases do not include the relevant LL states into the spectroscopic energy range.
34. Skinner, B.; Chen, T.; Shklovskii, B. I. Why Is the Bulk Resistivity of Topological Insulators So Small? *Phys. Rev. Lett.* **2012**, *109*, 176801.
35. Miller, D. L.; Kubista, K. D.; Rutter, G. M.; Ruan, M.; de Heer, W. A.; Kindermann, M.; First, P. N.; Stroscio, J. A. Real-Space Mapping of Magnetically Quantized Graphene States. *Nat. Phys.* **2010**, *6*, 811–817.
36. Hanaguri, T. Development of High-Field STM and Its Application to the Study on Magnetically-Tuned Criticality in $Sr_3Ru_2O_7$. *J. Phys.: Conf. Ser.* **2006**, *51*, 514–521.